Inhibition of HIF2 Prevents the Development of Neurodegenerative Disorder Induced by Deficiency of IRP2

Jiaqi Shen
Nanjing University Medical School
Li Xu
Nanjing University Medical School
Yuxuan Li
Nanjing University Medical School
Weichen Dong
Nanjing University Medical School Clinical College: East Region Military Command General Hospital
Jing Cai
Nanjing University Medical School Affiliated Nanjing Drum Tower Hospital
Yutong Liu
Nanjing University Medical School
Hongting Zhao
Nanjing University Medical School
Tianze Xu
Nanjing University Medical School Affiliated Nanjing Drum Tower Hospital
Esther Meyron Holtz
Technion Israel Institute of Technology
Yanzhong Chang
Hebei Normal University College of Life Sciences
Tong Qiao
Nanjing University Medical School Affiliated Nanjing Drum Tower Hospital
Kuanyu Li (likuanyu@nju.edu.cn)
Nanjing University https://orcid.org/0000-0001-9738-049X

Research

Keywords: iron regulatory protein 2, hypoxia inducible factor 2α, glycolysis, oxidative phosphorylation, iron–sulfur cluster, neurodegeneration

Posted Date: June 8th, 2021

DOI: https://doi.org/10.21203/rs.3.rs-529722/v1

Abstract

Background: IRP2 (Iron regulatory protein 2) deficiency in mice and humans causes microcytic anemia and neurodegeneration due to functional cellular iron depletion. Our previous in vitro data have demonstrated that Irp2 depletion upregulates hypoxia-inducible factor subunits Hif1α and Hif2α expression and inhibition of Hif2α rescues Irp2 ablation-induced mitochondrial dysfunction and inhibition of Hif1α suppresses the overdose production of lactic acid derived from actively aerobic glycolysis. We wonder whether Hif1α and Hif2α are also elevated in vivo, and if they are elevated, are they related to the neurodegenerative disorder of *Irp2*$^{-/-}$ mice.

Results: In this study, we confirmed the upregulated Hif2α, not Hif1α, in tissues, particularly, the central nervous system including the mainly affected cerebellum and spinal cord of *Irp2*$^{-/-}$ mice. Consistent with this observation, inhibition of Hif2α by PT-2385, not Hif1α by PX-478, prevented the neurodegenerative symptoms, which was proved by Purkinje cells arrangement from the shrunken and irregular to the full and regular array. PT-2385 treatment did not only modulate mitochondrial morphology and quality in vivo, but also suppressed the glycolysis. Consequently, the shift of energy metabolism from glycolysis to oxidative phosphorylation reversed.

Conclusions: Our results indicate that Irp2 depletion-induced Hif2α is alone, in vivo, in charge of the switch between oxidative phosphorylation and glycolysis, suggesting that, for the first time to our knowledge, Hif2α is a clinically potential target in the treatment of IRP2 deficiency-induced neurodegenerative syndrome.

1 Introduction

Iron is an indispensable element in mammals. Maintaining proper iron concentration in our body is of great significance because iron, in forms of heme, iron-sulfur cluster (Fe-S), or iron itself as important cofactors, are involved in multiple biochemical pathways, including hemoglobin synthesis and mitochondrial respiratory chain (Hentze et al., 2004; Darshan et al., 2010; Ganz and Nemeth, 2012; Rouault, 2013). For this reason, mammals have developed sophisticated mechanisms to maintain proper iron concentration in the body: (1) systemic iron homeostasis is maintained by hepcidin-ferroportin (hepcidin-FPN1, encoded by *HAMP* and *SCL40A1*) axis (Nemeth et al., 2004; Ganz and Nemeth, 2011); (2) cellular iron homeostasis is mediated by iron regulatory proteins (IRPs, IRP1 and IRP2, also called ACO1 and IREB2) through IRP-IRE (iron responsive element) system (Rouault, 2006; Wallander et al., 2006; Muckenthaler et al., 2008; Rouault, 2013). More tissue specific strategies have also been developed, e. g. ferritinophagy to regulate erythropoiesis (Mancias et al., 2015). These ways function and interplay to fine-tune iron levels in the body (Zhang et al., 2014).

IRP1 and IRP2 are both iron-regulatory RNA binding proteins that regulate the expression of a series of iron-related genes at the post-transcriptional levels (Hentze et al., 2010; Anderson et al., 2012). Under conditions of iron deficiency, the IRE in the target mRNA can be recognized and bound by IRPs, but the

consequence of IRP binding depends on the position of the IRE on the mRNA of the target genes. If the IRE is in the 5'-untranslated region (UTR) of the target mRNA, the binding of IRPs may inhibit the translation of the genes, including L- and H-ferritin and FPN1; if the IRE is in the 3'-UTR, the binding of IRPs may stabilize the mRNA, such as that of transferrin receptor 1 (TfR1) (Casey et al., 1988; Müllner et al., 1989) and divalent metal transporter 1 (DMT1) (Tybl et al., 2020). When cellular iron is sufficient, IRP1 binds to a [4Fe-4S] cluster, therefore, gains aconitase activity and loses the ability to bind IRE, whereas IRP2 is removed by iron and oxygen-mediated proteasome degradation (Salahudeen et al., 2009; Vashisht et al., 2009) to avoid the excessive iron uptake and to promptly stores excess intracellular iron and/or export excess iron.

Studies in animal models have shown that IRPs also play an important role in the regulation of systemic iron homeostasis. It has been reported that *Irp2*$^{-/-}$ mice suffer from microcytic anemia (Cooperman et al., 2005; Galy et al., 2005), neurologic defects (LaVaute et al., 2001; Jeong et al., 2011) and diabetes (Santos et al., 2020). The cause of these symptoms are considered to be lack of functional iron in erythroblast progenitors, the cells in central nervous system (CNS), and β cells of *Irp2*$^{-/-}$ mice. The patient with bi-allelic loss-of-function variants in the gene iron responsive element binding protein 2 (IREB2) leading to an absence of IRP2 also presented neurological and haematological features (Costain et al., 2019), similar, but much more severely, to the observation in *Irp2*$^{-/-}$ mice. The symptoms could be caused by the deficiency of Fe-S biogenesis, which further compromised the mitochondrial quality (Li et al., 2018; Li et al., 2019).

Recently, we found that mitochondrial dysfunction was closely associated with the reduced expression of a number of genes that are involved in Fe-S biogenesis and mitochondrial respiratory chain (Li et al., 2018). The further investigation revealed that Irp2 may function as a key to switch the metabolism between aerobic glycolysis and oxidative phosphorylation (OXPHOS), mediated by upregulation of hypoxia-inducible factor subunits Hif1α and Hif2α in mouse embryonic fibroblasts (MEFs) (Li et al., 2019). HIF1 and HIF2 are two important transcription factors that can regulate the expression of a series of genes. Active HIF is a heterodimer, composed of α subunit (HIF1α or Hif2α) and β subunit (HIF1β, also called ARNT) and can bind hypoxia responsive element (HRE), which is a very important mechanism in intestinal iron absorption (Mastrogiannaki et al., 2009; Shah et al., 2009) and under other conditions, such as cancer (Keith et al., 2011) and ischemia (Kapitsinou et al., 2014; Barteczek et al., 2017). IRP1 can bind to the IRE in the 5'-UTR of HIF2α mRNA to regulate HIF2α at the post-transcriptional level (Sanchez et al., 2007; Zimmer et al., 2008). In *Irp1*$^{-/-}$ mice, elevated Hif2α up-regulates erythropoietin (EPO), causing the mice to develop polycythemia and pulmonary hypertension (Anderson et al., 2013; Ghosh et al., 2013; Wilkinson and Pantopoulos, 2013). Interestingly, in *Irp2*$^{-/-}$ MEFs we found that Hif1α and Hif2α were both up-regulated, which switches the metabolism type from oxidative phosphorylation to glycolysis (Li et al., 2019). Inhibition of both Hif1α and Hif2α reversed the energy metabolism.

In this study, we confirmed the elevated Hif2α, not Hif1α, in *Irp2*$^{-/-}$ mice. The upregulated glycolytic pathway-related proteins were also observed and associated with the enhanced glycolysis, while down-

regulated frataxin (Fxn) and iron–sulfur cluster scaffold protein (IscU), respectively, were observed and associated with deficiency of iron-sulfur clusters. Consequently, the expression of electron transmit chain (ETC) subunits was reduced and OXPHOS was weakened. After the inhibition of Hif2α by PT-2385, the energy metabolism was shifted from glycolysis to OXPHOS in *Irp2*$^{-/-}$ mice, the histological and behavioral indicators were restored, and neurodegenerative symptoms were alleviated. Our results indicate that the neurodegenerative disorder induced by the loss of Irp2 is, at least partially, mediated by the upregulated Hif2α.

2 Materials And Methods

2.1 Mice

The *Irp2*$^{+/-}$ heterozygous mice were obtained by crossing the purchased *Irp2*$^{-/-}$ mice (Purchased from MMRRC at UC Davis, USA, Cat. No. 030490-MU) with WT C57/BL6 mice. Both *Irp2*$^{-/-}$ and WT mice used in the experiment were the descendants of *Irp2*$^{+/-}$ heterozygous mice. The mice were fed a standard rodent pellet diet (200 mg iron/kg) and maintained a constant 12-hour light/dark cycle. All procedures were carried out according to the NIH Guide for the Care and Use of Laboratory Animals and were approved by the Animal Experimentation Administration of Nanjing University.

2.2 Behavior Tests

2.2.1 Hang Tests Hang test was performed to assess the grip strength. In the hang test, mice were allowed to grip a wire mesh square that was then inverted. The latency time that mice could hang on to an inverted wire mesh square before falling was measured. And each mouse was tested for three times with an interval of 5 min.

2.2.2 Rotarod Tests The motor functions of balance and coordination were assessed using an accelerating rotarod (Jiangsu SANS Technology Co., Ltd.). Recorded the staying time of mice on the rotating rod (the rotating rod accelerated from 4 rpm to 40 rpm within 5 min), and each mouse was tested for three consecutive times.

2.3 Drug Treatment

Both PT-2385 and PX-478 were dissolved in DMSO, diluted with normal saline and injected intraperitoneally into six-month-old male *Irp2*$^{-/-}$ mice. The injection doses of PT-2385 and PX-478 were 0.4 mg/kg body weight and 5 mg/kg body weight, respectively, and the injections lasted for one month every other day.

2.4 Blood Routine Tests

The red blood cell (RBC), hemoglobin (HGB), hematocrit (HCT) and mean corpuscular volume (MCV) were detected by Mindray automatic hematology analyzer (BC-2800vet, Shenzhen, China).

2.5 H&E Staining

In H&E staining, tissue sections were dealt with the following steps: dewaxed for 10 min in xylene twice; hydrated for 5 min in each 100% − 50% ethanol gradient buffers; rinsed for 5 min in running water at room temperature; stained with Hematoxylin for 10 min, then in Eosin Y for 10 min. Slides were dehydrated through gradual ethyl alcohol solutions for imagining.

2.6 Electron Microscopy

The cerebellum and spinal cord were separated in the size of rice grains, placed in a mixed solution of 2% paraformaldehyde and 0.1 M cacodylate for 30 min at room temperature, then stored at a constant temperature of 4˚C (refrigerator). The samples were rinsed once or twice, then dehydrated through a series of ethanol from 50–100%, and then propylene oxide was used instead of ethanol. The samples were stored in 50% propylene oxide and 50% EPON resin (1:1 mix) for 1 hour, and then placed in pure EPON. The samples were transferred to fresh EPON in molds or beem embedding capsules, which were filled carefully to avoid air bubbles, and kept at 60˚C for at least 24 h. Samples were observed and photographed by using HT7800 electron microscope at 80 keV, and electron micrographs were commented by Hitachi TEM system.

2.7 Quantitative Real-time PCR (qRT-PCR)

Total RNA was isolated with RNA isolater Total RNA Extraction Reagent (Vazyme Nanjing, China), and cDNA was obtained by using HiScript® Ⅱ RT SuperMix for qPCR (+ gDNA wiper) (Vazyme Nanjing, China). qPCR operates by ChamQTM Universal SYBR® qPCR Master Mix (Vazyme Nanjing, China). The results were normalized against actin levels. The following primers were used: for actin, forward primer 5'-GCCACTGCCGCATCCTCTTC-3' and reverse primer 5'-AGCCTCAGGGCATCGGAACC-3'; for EPO, forward primer 5'-AGTTGCCTTCTTGGGACTGA-3' and reverse primer 5'-GCCACTCCTTCTGTGACTCC-3'; for Hepcidin, forward primer 5'-CTCCTGCTTCTCCTCCTTGC-3' and reverse primer 5'-GCAATGTCTGCCCTGCTTTC-3'; for endothelin-1 (Edn1), forward primer 5'-CCAGGCAGTTAGATGTCAGT-3' and reverse primer 5'-CCAGCTGCTGATAGATACAC-3'; for LdhA, forward primer 5'-ACTGTGTAACTGCGAACTCC-3' and reverse primer 5'-CCACGTAGGTCAAGATATCC-3'; for Glut1, forward primer 5'-AGGCTTGCTTGTAGAGTGAC-3' and reverse primer 5'-CAGTGTTATAGCCGAACTGC-3'; for Hk2, forward primer 5'-TGATCGCCTGCTTATTCACGG-3' and reverse primer 5'-AACCGCCTGAAATCTCCAGA-3'. The results were normalized against actin levels.

2.8 Western Blot Analysis

The total protein of each entire tissue was extracted and analyzed (25–35 μg total protein/lane) by 7.5%-12.5% SDS-PAGE at 100 V, transferred onto nitrocellulose membrane at 250 mA for 1.5 h, and analyzed by immunoblotting. The information of the primary antibody is as follows: anti-ferritin light chain (cat# 69090), Hif2α (cat# 109616), NcoA4 (cat# ab86707) and SdhB (cat# 178423) from Abcam (Cambridge, MA), anti-TfR (cat# 136800) from Zymed (San Francisco, CA), anti-beta-actin (cat# BM0627) from Boster (Wuhan, China), anti-HK2 (cat# 22029-1-AP), Glut1 (cat# 21829-1-AP), LdhA (cat# 19987-1-AP), Ndufs1 (cat# 12444-1-AP), and Uqcrfs1 (cat# 18443-1-AP) from Proteintech Group Inc. (Chicago, IN), anti-Hif1α (cat# 14179) from Cell Signaling Technology Inc. (Shanghai, China), anti-ferritin heavy chain

(cat# AJ1290b) from ABGENT (San Diego, CA), anti-Fxn, IscU, Irp1 and Irp2 (polyclonal, self-made, raised from rabbits). All the self-made antibodies were validated in previous studies (Li et al., 2018; Li et al., 2019). When it is necessary to detect multiple proteins in one blot and the molecular weight of the protein is different, we cut the blotted nitrocellulose membrane according to the molecular weight, and then incubate with different antibodies. When the molecular weights are very close, run multiple gels with the same prepared total protein samples, transfer them to nitrocellulose membranes, cut according to molecular weights, and then incubate with different antibodies. We used Tanon Science and Technology Co., Ltd. (Shanghai, China) ECL-plus reagent to visualize the detected proteins. The intensity of the western blot band was quantified by ImageJ software. Each experiment was repeated at least three times independently, and biological replicates were performed in parallel each time. The average intensity of the bands from replicate samples was first normalized to an internal control (actin), and then normalized to a wild-type control, with the value set to 1. The final value was the average value from at least three independent experiments.

2.9 Enzyme-Linked Immunosorbent Assay (ELISA)

The serum erythropoietin (EPO) and interleukin-6 (IL-6) levels were quantified using specific ELISA kits according to the manufacturers' instructions (Invitrogen).

2.10 Ferrozine Iron Assay

The serum, intestinal, cerebellum, and spinal cord iron content were detected by the Ferrozine Iron Assay. Took 50 μL lysate or serum (took double volume for lysis buffer as control). Added 11 μL concentrated HCL (11.6 M). Placed all tubes on the 95℃ heating block for 20 min. Centrifuged at the highest speed for 10 min, removed very gently from centrifuge. Removed 45 μL supernatant very carefully. Added 18 μL ascorbate (75 mM) to each tube, ascorbate acts as a reductant, moving Fe from 3^+ state to the 2^+ state. Vortex-quick spin, incubated for 2 min. Added 18 μL ferrozine (10 mM) to each tube. Ascorbate acts as an oxidant, taking Fe from the 2^+ state to the 3^+ state, incubated for 2 min. Added 36 μl saturate ammonium acetate (NH_4Ac) to each tube, incubated for 2 min. Read samples at 562 nm using multifunctional fluorescent microplate reader.

2.11 Enzymatic Activities

The activities of complex I and II were measured according to the manufacturer's protocols, respectively. Both kits were purchased from Comin Biotechnology Co. (Suzhou, Jiangsu, China).

2.12 Determination of ATP Content

The levels of ATP in tissues were detected by using ATP determination kit (Beyotime Biotech.). The reading is measured by GloMaxTM96-well plate luminescence detector (E6521)

2.13 Lactic Acid Production

The tissue lysates were collected and assayed according to the lactic acid production detection kit (Nanjing Jiancheng Bioengineering Institute). The assay was detected by multifunctional fluorescent microplate reader at 530 nm.

2.14 Statistical Analysis

Student's t-test or one-way analysis of variance (ANOVA) was carried out using Graphpad prism 8. The measurement was expressed as the mean ± SEM; all the experiments were repeated more than 3 times independently. Significance was considered at $p < 0.05$.

3 Results

3.1 Glycolysis-related gene expression is enhanced and OXPHOS-related gene expression is weakened in the CNS tissues of Irp2$^{-/-}$ mice

Our previous *in vitro* study demonstrated that metabolism switch took place from OXPHOS to glycolysis in *Irp2*$^{-/-}$ MEFs (Li et al., 2019). We wonder if it is the case *in vivo*. First, we detected the expression levels of iron-related proteins in the CNS tissues (cerebrum, cerebellum, brainstem and spinal cord) of *Irp2*$^{-/-}$ mice. Compared with that in wild type (WT) mice, ferritin expression was increased, while Tfr1 was decreased in *Irp2*$^{-/-}$ mice (Fig. 1A and B), which was in line with previous study (Jeong et al., 2011). Next, we detected the expression levels of Hif1α and glycolysis-related proteins and did not find the same elevation of Hif1α as we observed in *Irp2*$^{-/-}$ MEF (Li et al., 2019). However, glycolysis-related proteins, including lactate dehydrogenase A (LdhA), glucose transporter 1 (Glut1), hexokinase 2 (Hk2), were upregulated, compared with that in WT mice (Fig. 1C and D), although these genes are the members of Hif1 regulon. Then, we detected the expression levels of Hif2α, the Fe-S biogenesis-related proteins (IscU and Fxn), and mitochondrial respiratory complex subunits (Ndufs1, SdhB, and Uqcrfs1). We found that the levels of IscU and Fxn were reduced and subunits of complex I (Ndufs1), II (SdhB) and III (Uqcrfs1) were also reduced in the CNS tissues of *Irp2*$^{-/-}$ mice, compared with WT mice (Fig. 1E and F), suggesting a reduction of OXPHOS. Taken together, our results confirmed the biochemical changes *in vivo* related to energy metabolism, OXPHOS and glycolysis, in the tissues of the CNS of *Irp2*$^{-/-}$ mice.

3.2 Administration of PT-2385 significantly improves the behavioral performance and anemia of Irp2$^{-/-}$ mice

As presented above, we only observed the upregulation of Hif2α in central nervous tissues of *Irp2*$^{-/-}$ mice, but both inhibitors, PX-478 (5 mg/kg body weight) for Hif1α and PT-2385 (0.4 mg/kg) for Hif2α, were still injected into *Irp2*$^{-/-}$ mice intraperitoneally every other day for one month, individually. During the one month, the mice weight was all monitored and found increased normally without difference compared with the vehicle treatment, indicating the safety of the drug and its dosage (Fig. 2A). In terms of behavioral performance, the latency time of *Irp2*$^{-/-}$ mice on the rotating rod and the hanging time on the

wire mesh square were significantly shorter than that of the WT mice. However, it significantly recovered in *Irp2*$^{-/-}$ mice after administration of PT-2385, while no efficacy was observed after PX-478 treatment in agreement with no change of Hif1α levels in the CNS tissues of mutant mice (Fig. 2B and *C*). To confirm the effect of PT-2385 in *Irp2*$^{-/-}$ mice is through rescuing Irp2 deficiency, we also treated the WT mice with PT-2385. The rotarod and hang tests did not show the significant difference between the vehicle and PT-2385 treatment (not shown). These data proved the critical role of Hif2α in CNS of *Irp2*$^{-/-}$ mice. Since then, our work focused on Hif2α inhibition by PT-2385.

The anemia of *Irp2*$^{-/-}$ mice, likely, resulted from decreased expression of TfR1 in erythroblasts and decreased bone marrow iron stores (Cooperman et al., 2005; Galy et al., 2005). Very interestingly, PT-2385 treatment corrected the anemia of *Irp2*$^{-/-}$ mice as well, showing reversed number of red blood cells, hemoglobin, and hematocrit, but not the mean corpuscular volume (Fig. 2D, E, F and G). Then, we measured more parameters to evaluate the iron status, including the *EPO* mRNA in kidney, serum EPO and iron. Surprisingly, the iron status globally improved (Fig. 2H, I and J). To understand how the PT-2385 treatment corrected the iron insufficiency anemia of *Irp2*$^{-/-}$ mice, we assessed the iron content in intestine and liver, *HAMP* mRNA level in liver, and serum interleukin 6 to determine whether the serum iron resulted from intestinal uptake or iron release from liver. The results showed that *HAMP* mRNA levels in liver, and serum interleukin 6 (IL-6), and iron content in intestine and liver all reduced after PT-2385 treatment (Fig. 2K, L, M and N), suggesting that both ways, intestinal uptake and iron release from liver, contributed to the elevation of the serum iron. This assumption was further supported by the increased NcoA4 (Fig. 2O and P), which is involved in ferritinophagy for ferritin degradation to release iron (Mancias et al., 2014).

3.3 The administration of PT-2385 protects the histological morphology and mitochondrial ultrastructure in spinal cord and cerebellum of Irp2$^{-/-}$ mice

Previous studies have demonstrated that misregulation of iron metabolism from loss of *Irp*2 causes neuronal degeneration and mitochondrial dysmorphology (Jeong et al., 2011). Cerebellum and spinal cord are among the most severely affected tissues, so we examined them hereinafter. The hematoxylin-eosin staining (H&E) staining revealed that cerebellar Purkinje cells were full, intact, and tightly arranged in line in WT mice, while they were severely shrunk and/or missing in *Irp2*$^{-/-}$ mice. However, PT-2385 treatment significantly suppressed the cerebellar Purkinje cells from degeneration or loss in *Irp2*$^{-/-}$ mice (Fig. 3A). The results from the electron microscopy showed that the density of mitochondria in mutant cerebellum is lightened, which phenomenon was much more severe in the spinal cord of *Irp2*$^{-/-}$ mice than that in WT mice. More affectedly, the morphology of the mitochondria in spinal cord of *Irp2*$^{-/-}$ mice became swollen, vacuolated, and internal-cristae damaged. Interestingly, PT-2385 treatment significantly alleviated the poor presentation, including the deformed mitochondria and Wallerian and segmental demyelination (Fig. 3B, C and D), suggesting the beneficial effect of PT-2385 against motor neurodegeneration.

3.4 Inhibition of Hif2α effectively rescues the weakened OXPHOS in the cerebellum and spinal cord of Irp2$^{-/-}$ mice

According to the results in Fig. 1 and previous studies (Li et al., 2018; Li et al., 2019), *Irp2* depletion induced mitochondrial dysfunction via reduction of Fe-S biogenesis. We evaluated the levels of Fxn and IscU and of complex subunits, Ndufs1, SdhB and Uqcrfs1, in the tissues, cerebellum and spinal cord, of *Irp2*$^{-/-}$ mice. Again, Hif2α was found increased and the expression of mitochondrial proteins, including Fxn, IscU, and complex subunits, was decreased in *Irp2*$^{-/-}$ mice compared with WT. However, PT-2385 treatment inhibited all these biochemical changes compared with *Irp2*$^{-/-}$ mice (Fig. 4A, B, C and D). In line with these results, the activities of mitochondrial complex I and II were also significantly restored in both tissues (Fig. 4E and F). The exception is the coupled ETC product ATP. In cerebellum, ATP content was lower in *Irp2*$^{-/-}$ mice than that in WT mice and PT-2385 administration increased it, which is correlated with the ETC activities (Fig. 4G). However, in spinal cord, ATP content increased significantly in *Irp2*$^{-/-}$ mice (Fig. 4H), which is consistent with the previous studies (Li et al., 2018; Li et al., 2019) in MEFs though the ETC-related proteins and enzymatic activities were lower in *Irp2*$^{-/-}$ mice than those in WT mice (Fig. 4C, D and F). The reason will be discussed further in Discussion. Very surprisingly, compared with *Irp2*$^{-/-}$ mice, more ATP was produced after PT-2385 administration (Fig. 4H). Overall, the inhibition of Hif2α by PT-2385 rescues the weakened OXPHOS in *Irp2*$^{-/-}$ mice to provide more ATP to fulfill the energy need.

3.5 Inhibition of Hif2α attenuates enhanced glycolysis in the cerebellum and spinal cord of Irp2$^{-/-}$ mice

Though Hif1α was not found to be upregulated *in vivo*, we observed the enhanced glycolysis-related gene expression (Fig. 1B), which is similar to the previous results in *Irp2*$^{-/-}$ MEFs (Li et al., 2019). We still used the tissues cerebellum and spinal cord to check the effect of PT-2385 on the expression of *LdhA*, *Glut1, Hk2*, and *endothelin 1* (*Edn1*), which genes are considered to be the members of Hif regulon. The results showed that the expression of these genes increased in *Irp2*$^{-/-}$ mice and reduced to the WT levels after PT-2385 treatment (Fig. 5A and B), confirming the action of PT-2385 on Hif2α and the regulon relationship of Hif2α to the tested genes. The protein levels of glycolysis-related genes including LdhA, Glut1, and Hk2 were also significantly reduced after PT-2385 treatment (Fig. 5C, D, E and F). Accordingly, the lactic acid levels were significantly higher in both cerebellum and spinal cord of *Irp2*$^{-/-}$ mice than those in WT, and PT-2385-treatment significantly lowered the levels in both tissues of *Irp2*$^{-/-}$ mice (Fig. 5G and H). Comparing the two tissues, cerebellum and spinal cord, the upregulated Hif targeted genes seemingly responded stronger in spinal cord than in cerebellum since their mRNA levels elevated more in spinal cord (Fig. 5B) than in cerebellum (Fig. 5A), particularly for *Hk2* and *Edn1*, after Irp2 depletion. The protein levels of LdhA and Glut1 in the spinal cord increased about twofold and fivefold, respectively (Fig. 5E and F), versus 1.3- and 2-fold in the cerebellum (Fig. 5C and D) after Irp2 depletion. The results suggest that the spinal cord might suffer more from the upregulated Hif2α and active glycolysis.

4 Discussion

In this study, we found that Irp2 ablation-induced Hif2α upregulation alone mediated the metabolism switch from OXPHOS to glycolysis *in vivo*. The protective effect of PT-2385 through Hif2α inhibition suggested that Hif2α is a potential target therapeutically in the treatment of IRP2 mutant-caused neurodegenerative syndrome.

Irp2 depletion causes the deficiency of cellular functional iron by decreasing transferrin receptor and increasing ferritin expression (Jeong et al., 2011), which compromise the heme biosynthesis and finally trigger microcytic anemia in mice (Cooperman et al., 2005; Galy et al., 2005) and in humans (Cooper et al., 2019; Costain et al., 2019). Both the functional iron deficiency and anemia-induced low oxygen tension/hypoxia could upregulate Hif1α and/or Hif2α expression *in vivo*. In our previous study, we did find that Irp2 ablation induced the increase of Hif1α and Hif2α in *Irp2*$^{-/-}$ MEFs (Li et al., 2019). However, we did not find the increase of Hif1α, but Hif2α in *Irp2*$^{-/-}$ mice. Inhibition of Hif2α by PT-2385 greatly alleviated the progress of neurodegeneration through the enhancement of mitochondrial Fe-S biogenesis and suppression of glycolytic pathway-related proteins. In agreement with previous study in vitro (Li et al., 2018; Li et al., 2019), the loss of *Irp*2 in mice downregulated the expression of Fxn and IscU, two important core components in Fe-S biogenesis machinery. Increase of Fxn and IscU in *Irp2*$^{-/-}$ cells, either by overexpression of the two genes (Li et al., 2018) or by inhibition of Hif2α (ref.(Li et al., 2019) and this study), augments the mitochondrial complex activities and ATP content. At the same time, inhibition of Hif2α also weakened glycolysis to avoid the toxicity of high levels of lactic acid through suppression of *LdhA*, *Glut1*, and *Hk2*. Therefore, PT-2385 administration dramatically protected from the progressive neurodegeneration as modeled in Fig. 6.

Interestingly, Hif2 inhibition also improved blood parameters overall from anemia. However, Hif2 is very important for erythropoiesis by regulating EPO production and for iron uptake in the small intestine by regulating DMT1, FPN1 and Dcytb. Surprisingly, we found that the lifted iron content in liver of *Irp*2 mutant reduced and the increased ferritin dropped back to WT levels. More profoundly, we found that NcoA4 expression increased in liver after Hif2 inhibition, suggesting the important role of NcoA4 for iron release from ferritin, very likely, through ferritinophagy.

Both Hif1α and Hif2α are regulated by oxygen and iron (Majmundar et al., 2010; Prabhakar and Semenza, 2012). In this study, we found the elevated Hif2α alone, not together with Hif1α, contribute to the switch of energy metabolism from OXPHOS to glycolysis. The rationale for Hif2α to regulate IscU has been demonstrated that IscU is a member of the miR-210 regulon (Chan et al., 2009) and the promoter of miR-210 contains a HRE for Hif1/2 binding (Kulshreshtha et al., 2007). Therefore, down-regulation of IscU may be explained to be through the miR-210-Hif2 axis in *Irp2*$^{-/-}$ mice. The accompanied co-regulation of Fxn with IscU was often observed (Ferecatu et al., 2018; Li et al., 2018; Li et al., 2019), the detail regulation mechanism of Hif2α on Fxn remains to be explored. If mouse Fxn was regulated by Hif2α as reported (Oktay et al., 2007), it would expect that Fxn expression should be increased. Indeed, Irp2 depletion induced the downregulation of Fxn, which expression was reversed after inhibition of Hif2α by PT-2385.

The co-regulation of Fxn and IscU could be the key to response to PT-2385 treatment since the interaction of Fxn with IscU is important to facilitate Fe-S biogenesis (Fox et al., 2019; Gervason et al., 2019) to cure mitochondrial dysfunction. The similar work has been reported that neuronal Hif1α and Hif2α deficiency improves neuronal survival and sensorimotor function in the early acute phase after ischemic stroke (Barteczek et al., 2017).

Though the 5'-UTR of *Hif2α* mRNA contains an IRE element for Irp1 binding (Sanchez et al., 2007; Barteczek et al., 2017), Irp1-IRE binding activity keeps constant in Irp2 depletion tissues (Zumbrennen-Bullough et al., 2014). Hif2α is, likely, upregulated by iron deficiency and anemia-induced hypoxia in *Irp2*$^{-/-}$ mice as discussed above. Interestingly, *Irp1*$^{-/-}$-induced elevated Hif2α up-regulates EPO, causing the mice to develop polycythemia and pulmonary hypertension (Anderson et al., 2013; Ghosh et al., 2013; Wilkinson and Pantopoulos, 2013). However, the upregulated EPO expression in *Irp2*$^{-/-}$ mice is probably invalid due to the iron limit in bone marrow (Cooperman et al., 2005). Moreover, the increased Hif2α endowed glycolysis-related genes, such as *LdhA*, *Glut1*, and *Hk2*, in the cerebellum and spinal cord of *Irp*2$^{-/-}$ mice. Therefore, inhibition of Hif2 by PT-2385 did not only increase the expression of Fxn and IscU to strengthen mitochondrial function, but also decrease the expression of *LdhA*, *Glut1*, and *Hk2* to weaken glycolysis to avoid the toxicity of high level of lactic acid. Although according to the astrocyte-neuron lactate shuttle hypothesis, lactic acid can be used as an energy metabolism substrate for neurons, Irp2 deficiency-induced mitochondrial dysfunction is insufficient to meet the energy needs of neurons. Intriguingly, the elevated lactic acid was more in the spinal cord than in the cerebellum, which is consistent with the more severity in motor than in other behaviors (Jeong et al., 2011). The enhanced glycolysis could be the reason why the ATP production was slightly, but significantly, more in the spinal cord than in cerebellum after *Irp*2 ablation.

The patient with absence of IRP2 shows functional iron deficiency and mitochondrial dysfunction that emulate *Irp2*$^{-/-}$ mice (Costain et al., 2019). The complete loss of IRP2 in patient-derived lymphoblasts also induces the decreased expression of complex subunits and activities of mitochondrial complex I and II (Costain et al., 2019), although the expression levels of Hifs, FXN, ISCU and glycolytic pathway-related proteins are not detected. We expect that Hif2α is upregulated in the tissues of CNS in patients as we observed in *Irp2*$^{-/-}$ mice and the inhibition of Hif2 may be a therapeutic option for the IRP2-loss patients.

5 Conclusion

In summary, we have demonstrated that Irp2 ablation induces the expression of Hif2α, not Hif1α, in the tissues of CNS of *Irp2*$^{-/-}$ mice and inhibition of Hif2α by PT-2385 dramatically protects from the neurodegenerative disorder through shifting the energy metabolism from glycolysis to oxidative phosphorylation, indicating that Hif2α is a potential target for neurodegenerative syndrome caused by loss of IRP2.

Declarations

6 Ethics approval and consent to participate

The experimental procedures were carried out in accordance with the National Institutes of Health Guide for the Care and Use of Laboratory Animals, and were approved by the Institutional Animal Care and Use Committee at Nanjing Drum Tower Hospital. No human studies are presented in this manuscript.

7 Consent for publication

Not applicable.

8 Availability of data and materials

The datasets used or analysed during the current study are available from the corresponding author on reasonable request.

9 Competing interests

The authors declare no competing interests.

10 Funding

This study was supported by grants from the National Basic Research Program of China (Grant 2015CB856300) and by the National Natural Science Foundation of China (Grants 31871201 and 31571218).

11 Authors' contributions

Conceptualization, Jiaqi Shen, Esther Meyron-Holtz, Tong Qiao and Kuanyu Li; Formal analysis, Jiaqi Shen; Funding acquisition, Tong Qiao and Kuanyu Li; Investigation, Jiaqi Shen, Li Xu, Yuxuan Li, Weichen Dong, Yutong Liu, Hongting Zhao and Tianze Xu; Methodology, Jiaqi Shen, Li Xu, Jing Cai, Tianze Xu and Kuanyu Li; Project administration, Jiaqi Shen and Kuanyu Li; Resources, Yanzhong Chang; Validation, Jiaqi Shen, Yuxuan Li and Yutong Liu; Visualization, Jiaqi Shen; Writing – original draft, Jiaqi Shen and Kuanyu Li; Writing – review & editing, Jiaqi Shen and Kuanyu Li.

12 Acknowledgements

We thank Dr. Longcheng Shang for technical assistance.

References

1. Anderson CP, Shen M, Eisenstein RS, Leibold EA. Mammalian iron metabolism and its control by iron regulatory proteins. Biochim Biophys Acta. 2012;1823:1468–83.
2. Anderson SA, Nizzi CP, Chang Y-I, Deck KM, Schmidt PJ, Galy B, Damnernsawad A, Broman AT, Kendziorski C, Hentze MW, Fleming MD, Zhang J, Eisenstein RS. The IRP1-HIF-2α axis coordinates iron and oxygen sensing with erythropoiesis and iron absorption. Cell Metab. 2013;17:282–90.

3. Barteczek P, Li L, Ernst A-S, Böhler L-I, Marti HH, Kunze R. Neuronal HIF-1α and HIF-2α deficiency improves neuronal survival and sensorimotor function in the early acute phase after ischemic stroke. J Cereb Blood Flow Metab. 2017;37:291–306.
4. Casey JL, Hentze MW, Koeller DM, Caughman SW, Rouault TA, Klausner RD, Harford JB. Iron-responsive elements: regulatory RNA sequences that control mRNA levels and translation. Science. 1988;240:924–8.
5. Chan SY, Zhang Y-Y, Hemann C, Mahoney CE, Zweier JL, Loscalzo J. MicroRNA-210 controls mitochondrial metabolism during hypoxia by repressing the iron-sulfur cluster assembly proteins ISCU1/2. Cell Metab. 2009;10:273–84.
6. Cooper MS, Stark Z, Lunke S, Zhao T, Amor DJ. IREB2-associated neurodegeneration. Brain. 2019;142:e40.
7. Cooperman SS, Meyron-Holtz EG, Olivierre-Wilson H, Ghosh MC, McConnell JP, Rouault TA. Microcytic anemia, erythropoietic protoporphyria, and neurodegeneration in mice with targeted deletion of iron-regulatory protein 2. Blood. 2005;106:1084–91.
8. Costain G, Ghosh MC, Maio N, Carnevale A, Si YC, Rouault TA, Yoon G. Absence of iron-responsive element-binding protein 2 causes a novel neurodegenerative syndrome. Brain. 2019;142:1195–202.
9. Darshan D, Frazer DM, Anderson GJ. Molecular basis of iron-loading disorders. Expert Rev Mol Med. 2010;12:e36.
10. Ferecatu I, Canal F, Fabbri L, Mazure NM, Bouton C, Golinelli-Cohen M-P. Dysfunction in the mitochondrial Fe-S assembly machinery leads to formation of the chemoresistant truncated VDAC1 isoform without HIF-1α activation. PLoS One. 2018;13:e0194782.
11. Fox NG, Yu X, Feng X, Bailey HJ, Martelli A, Nabhan JF, Strain-Damerell C, Bulawa C, Yue WW, Han S. Structure of the human frataxin-bound iron-sulfur cluster assembly complex provides insight into its activation mechanism. Nat Commun. 2019;10:2210.
12. Galy B, Ferring D, Minana B, Bell O, Janser HG, Muckenthaler M, Schümann K, Hentze MW. Altered body iron distribution and microcytosis in mice deficient in iron regulatory protein 2 (IRP2). Blood. 2005;106:2580–9.
13. Ganz T, Nemeth E. Hepcidin and disorders of iron metabolism. Annu Rev Med. 2011;62:347–60.
14. Ganz T, Nemeth E. Iron metabolism: interactions with normal and disordered erythropoiesis. Cold Spring Harb Perspect Med. 2012;2:a011668.
15. Gervason S, Larkem D, Mansour AB, Botzanowski T, Müller CS, Pecqueur L, Le Pavec G, Delaunay-Moisan A, Brun O, Agramunt J, Grandas A, Fontecave M, Schünemann V, Cianférani S, Sizun C. Physiologically relevant reconstitution of iron-sulfur cluster biosynthesis uncovers persulfide-processing functions of ferredoxin-2 and frataxin. Nat Commun. 2019;10:3566. B) .
16. Ghosh MC, Zhang D-L, Jeong SY, Kovtunovych G, Ollivierre-Wilson H, Noguchi A, Tu T, Senecal T, Robinson G, Crooks DR, Tong W-H, Ramaswamy K, Singh A, Graham BB, Tuder RM, Yu Z-X, Eckhaus M, Lee J, Springer DA, Rouault TA. Deletion of iron regulatory protein 1 causes polycythemia and

pulmonary hypertension in mice through translational derepression of HIF2α. Cell Metab. 2013;17:271–81.

17. Hentze MW, Muckenthaler MU, Andrews NC. Balancing acts: molecular control of mammalian iron metabolism. Cell. 2004;117:285–97.
18. Hentze MW, Muckenthaler MU, Galy B, Camaschella C. Two to tango: regulation of Mammalian iron metabolism. Cell. 2010;142:24–38.
19. Jeong SY, Crooks DR, Wilson-Ollivierre H, Ghosh MC, Sougrat R, Lee J, Cooperman S, Mitchell JB, Beaumont C, Rouault TA. Iron insufficiency compromises motor neurons and their mitochondrial function in Irp2-null mice. PLoS One. 2011;6:e25404.
20. Kapitsinou PP, Sano H, Michael M, Kobayashi H, Davidoff O, Bian A, Yao B, Zhang M-Z, Harris RC, Duffy KJ, Erickson-Miller CL, Sutton TA, Haase VH. Endothelial HIF-2 mediates protection and recovery from ischemic kidney injury. J Clin Invest. 2014;124:2396–409.
21. Keith B, Johnson RS, Simon MC. (2011) HIF1α and HIF2α: sibling rivalry in hypoxic tumour growth and progression. Nat Rev Cancer 12.
22. Kulshreshtha R, Ferracin M, Wojcik SE, Garzon R, Alder H, Agosto-Perez FJ, Davuluri R, Liu C-G, Croce CM, Negrini M, Calin GA, Ivan M. A microRNA signature of hypoxia. Mol Cell Biol. 2007;27:1859–67.
23. LaVaute T, Smith S, Cooperman S, Iwai K, Land W, Meyron-Holtz E, Drake SK, Miller G, Abu-Asab M, Tsokos M, Switzer R, Grinberg A, Love P, Tresser N, Rouault TA. Targeted deletion of the gene encoding iron regulatory protein-2 causes misregulation of iron metabolism and neurodegenerative disease in mice. Nat Genet. 2001;27:209–14.
24. Li H, Zhao H, Hao S, Shang L, Wu J, Song C, Meyron-Holtz EG, Qiao T, Li K. Iron regulatory protein deficiency compromises mitochondrial function in murine embryonic fibroblasts. Sci Rep. 2018;8:5118.
25. Li H, Liu Y, Shang L, Cai J, Wu J, Zhang W, Pu X, Dong W, Qiao T, Li K. Iron regulatory protein 2 modulates the switch from aerobic glycolysis to oxidative phosphorylation in mouse embryonic fibroblasts. Proc Natl Acad Sci U S A. 2019;116:9871–6.
26. Majmundar AJ, Wong WJ, Simon MC. Hypoxia-inducible factors and the response to hypoxic stress. Mol Cell. 2010;40:294–309.
27. Mancias JD, Wang X, Gygi SP, Harper JW, Kimmelman AC. Quantitative proteomics identifies NCOA4 as the cargo receptor mediating ferritinophagy. Nature. 2014;509:105–9.
28. Mancias JD, Pontano Vaites L, Nissim S, Biancur DE, Kim AJ, Wang X, Liu Y, Goessling W, Kimmelman AC, Harper JW. (2015) Ferritinophagy via NCOA4 is required for erythropoiesis and is regulated by iron dependent HERC2-mediated proteolysis. Elife 4.
29. Mastrogiannaki M, Matak P, Keith B, Simon MC, Vaulont S, Peyssonnaux C. HIF-2alpha, but not HIF-1alpha, promotes iron absorption in mice. J Clin Invest. 2009;119:1159–66.
30. Muckenthaler MU, Galy B, Hentze MW. Systemic iron homeostasis and the iron-responsive element/iron-regulatory protein (IRE/IRP) regulatory network. Annu Rev Nutr. 2008;28:197–213.

31. Müllner EW, Neupert B, Kühn LC. A specific mRNA binding factor regulates the iron-dependent stability of cytoplasmic transferrin receptor mRNA. Cell. 1989;58:373–82.
32. Nemeth E, Tuttle MS, Powelson J, Vaughn MB, Donovan A, Ward DM, Ganz T, Kaplan J. Hepcidin regulates cellular iron efflux by binding to ferroportin and inducing its internalization. Science. 2004;306:2090–3.
33. Oktay Y, Dioum E, Matsuzaki S, Ding K, Yan L-J, Haller RG, Szweda LI, Garcia JA. Hypoxia-inducible factor 2alpha regulates expression of the mitochondrial aconitase chaperone protein frataxin. J Biol Chem. 2007;282:11750–6.
34. Prabhakar NR, Semenza GL. (2012) Adaptive and maladaptive cardiorespiratory responses to continuous and intermittent hypoxia mediated by hypoxia-inducible factors 1 and 2. Physiol Rev 92.
35. Rouault TA. The role of iron regulatory proteins in mammalian iron homeostasis and disease. Nat Chem Biol. 2006;2:406–14.
36. Rouault TA. Iron metabolism in the CNS: implications for neurodegenerative diseases. Nat Rev Neurosci. 2013;14:551–64.
37. Salahudeen AA, Thompson JW, Ruiz JC, Ma H-W, Kinch LN, Li Q, Grishin NV, Bruick RK. An E3 ligase possessing an iron-responsive hemerythrin domain is a regulator of iron homeostasis. Science. 2009;326:722–6.
38. Sanchez M, Galy B, Muckenthaler MU, Hentze MW. Iron-regulatory proteins limit hypoxia-inducible factor-2alpha expression in iron deficiency. Nat Struct Mol Biol. 2007;14:420–6.
39. Santos MCFD, Anderson CP, Neschen S, Zumbrennen-Bullough KB, Romney SJ, Kahle-Stephan M, Rathkolb B, Gailus-Durner V, Fuchs H, Wolf E, Rozman J, de Angelis MH, Cai WM, Rajan M, Hu J, Dedon PC, Leibold EA. Irp2 regulates insulin production through iron-mediated Cdkal1-catalyzed tRNA modification. Nat Commun. 2020;11:296.
40. Shah YM, Matsubara T, Ito S, Yim S-H, Gonzalez FJ. Intestinal hypoxia-inducible transcription factors are essential for iron absorption following iron deficiency. Cell Metab. 2009;9:152–64.
41. Tybl E, Gunshin H, Gupta S, Barrientos T, Bonadonna M, Celma Nos F, Palais G, Karim Z, Sanchez M, Andrews NC, Galy B. Control of Systemic Iron Homeostasis by the 3' Iron-Responsive Element of Divalent Metal Transporter 1 in Mice. Hemasphere. 2020;4:e459.
42. Vashisht AA, Zumbrennen KB, Huang X, Powers DN, Durazo A, Sun D, Bhaskaran N, Persson A, Uhlen M, Sangfelt O, Spruck C, Leibold EA, Wohlschlegel JA. Control of iron homeostasis by an iron-regulated ubiquitin ligase. Science. 2009;326:718–21.
43. Wallander ML, Leibold EA, Eisenstein RS. Molecular control of vertebrate iron homeostasis by iron regulatory proteins. Biochim Biophys Acta. 2006;1763:668–89.
44. Wilkinson N, Pantopoulos K. IRP1 regulates erythropoiesis and systemic iron homeostasis by controlling HIF2α mRNA translation. Blood. 2013;122:1658–68.
45. Zhang D-L, Ghosh MC, Rouault TA. The physiological functions of iron regulatory proteins in iron homeostasis - an update. Front Pharmacol. 2014;5:124.

46. Zimmer M, Ebert BL, Neil C, Brenner K, Papaioannou I, Melas A, Tolliday N, Lamb J, Pantopoulos K, Golub T, Iliopoulos O. Small-molecule inhibitors of HIF-2a translation link its 5'UTR iron-responsive element to oxygen sensing. Mol Cell. 2008;32:838–48.
47. Zumbrennen-Bullough KB, Becker L, Garrett L, Hölter SM, Calzada-Wack J, Mossbrugger I, Quintanilla-Fend L, Racz I, Rathkolb B, Klopstock T, Wurst W, Zimmer A, Wolf E, Fuchs H, Gailus-Durner V, de Angelis MH, Romney SJ, Leibold EA. Abnormal brain iron metabolism in Irp2 deficient mice is associated with mild neurological and behavioral impairments. PLoS One. 2014;9:e98072.

Figures

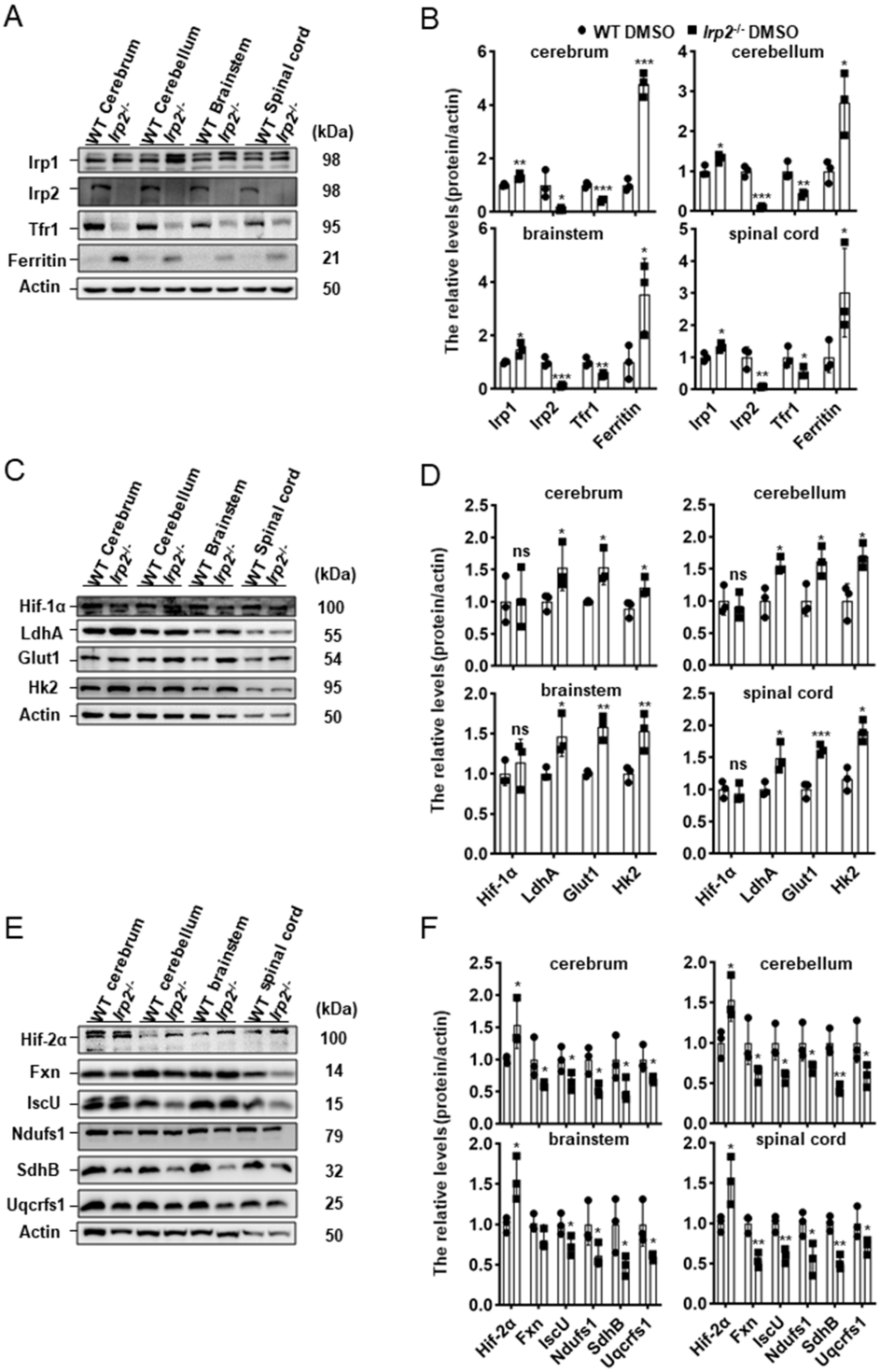

Figure 1

Irp2 ablation enhances glycolysis-related gene expression and diminishes OXPHOS-related gene expression in the tissues of CNS, analyzed by Western blots. (A) Protein levels of iron-related genes (Irp1, Irp2, Tfr1 and ferritin) in central nervous tissues (cerebrum, cerebellum, brainstem and spinal cord) of WT and Irp2-/- mice. (B) Quantification of the band intensity for (A). (C) Protein levels of hypoxia-inducible factor 1α (Hif-1α) and glycolytic pathway-related proteins (Glut1, Hk2 and LdhA) in central nervous

tissues (cerebrum, cerebellum, brainstem and spinal cord) of WT and Irp2-/- mice. (D) Quantification of the band intensity for (C). (E) Protein levels of hypoxia-inducible factor 2α (Hif-2α), Fe–S biogenesis-related genes (Fxn and IscU) and mitochondrial complex subunits (Ndufs1 for complex I, SdhB for complex II and Uqcrfs1 for complex III). (F) Quantification of the band intensity for (E). Actin was used as a loading control. Values represented as the mean ± SEM (n=3), and Student's T-test was used for statistics to evaluate the group differences. In B, D and F, *P <0.05, **P <0.01, ***P <0.001, Irp2-/- mice vs. WT mice.

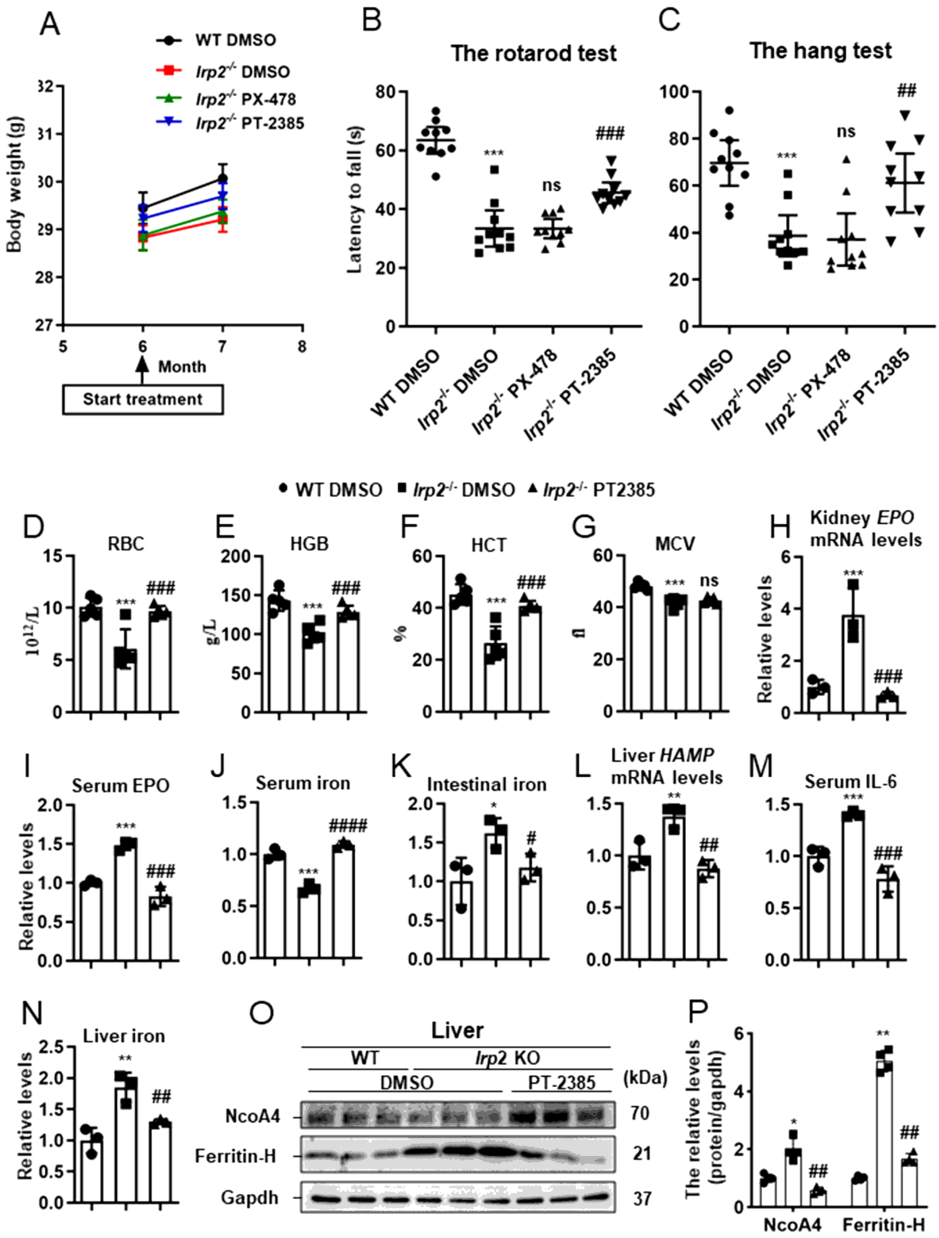

Figure 2

The administration of Hif2α inhibitor PT-2385, not Hif1α inhibitor PX-478, improves the behavioral performance and corrects anemia of Irp2-/- mice. Mice were divided into four groups: WT mice with vehicle (DMSO) administration (WT DMSO), Irp2-/- mice with DMSO administration (Irp2-/- DMSO), Irp2-/- mice with PT-2385 administration (Irp2-/- PT-2385), Irp2-/- mice with PX-478 administration (Irp2-/- PX-478). (A) The weight of mice before and after the drug administration. (B, C) The behavioral tests of mice, including the rotarod tests (B) and the hang tests (C), values are represented as the mean ± SEM (n=10). (D) Number of the red blood cells (RBC). (E) Hemoglobin concentration (HGB). (F) Hematocrit (HCT). (G) Mean corpuscular volume (MCV). (H) EPO mRNA levels in kidneys. (I) Serum EPO protein levels detected by ELISA. (J, K) Serum and intestinal iron content detected by the Ferrozine Iron Assays. (L) Hamp mRNA levels in livers. (M) Serum interleukin 6 (IL-6) protein levels detected by ELISA. (N) Liver iron content detected by the Ferrozine Iron Assays. (O) Protein levels of NcoA4 and ferritin-H in the liver detected by Western blot analysis. Gapdh was used as an internal control. (P) Quantification of the band intensity for (O). From D to P, n=3-5. The ANOVA was used for statistics to evaluate the group differences. In B-N and P, *P <0.05, **P <0.01, ***P <0.001, Irp2-/- DMSO vs. WT DMSO; #P <0.05, ##P <0.01, ###P <0.001, ####P <0.0001, Irp2-/- PT-2385 vs. Irp2-/- DMSO; ns P>0.05, Irp2-/- PX-478 vs. Irp2-/- and Irp2-/- PT-2385 vs. Irp2-/- DMSO.

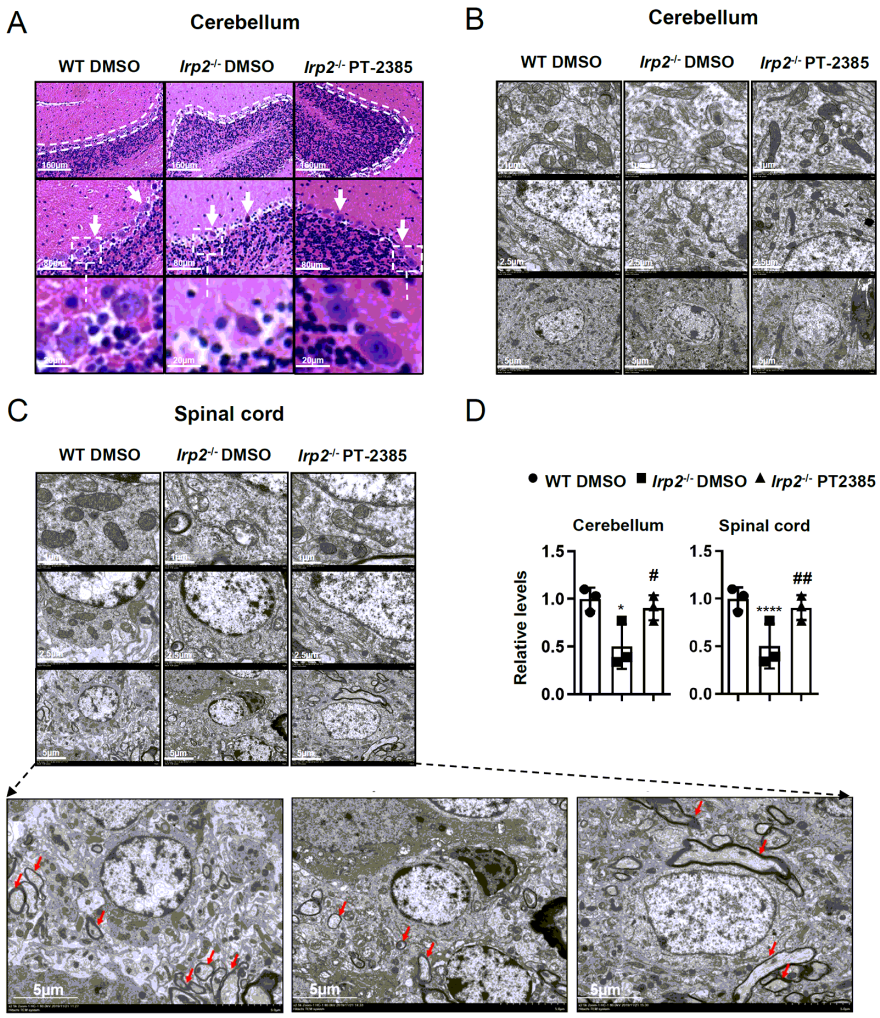

Figure 3

The histological morphology and mitochondrial ultrastructure in spinal cord and cerebellum of Irp2-/- mice are improved after PT-2385 administration. (A) The H&E stained sections of the cerebellum of WT DMSO, Irp2-/- DMSO, and Irp2-/- PT-2385 mice. The dotted lines indicate Purkinje cell layers (Top), and the arrows point to Purkinje cells (Middle). The Purkinje cells framed by the dotted line are magnified four times (Bottom). The scale bars are 160 μm, 80 μm, and 20 μm, respectively. (B, C) Transmission electron

micrographs of the cerebellum (B) and spinal cord (C) of WT DMSO, Irp2-/- DMSO, and Irp2-/- PT-2385 mice. The scale bars are 1 μm, 2.5 μm, and 5 μm, respectively. The bottom panel are magnified images myelin sheath and anonal degeneration. (D) The quantification of normal mitochondria (relative ratio comparing with that in WT). Values represented the mean ± SEM, n=3. The ANOVA was used for statistics to evaluate the group differences. *P <0.05, ****P <0.0001, Irp2-/- DMSO vs. WT DMSO; #P <0.05 and ##P <0.01, Irp2-/- PT-2385 vs. Irp2-/- DMSO.

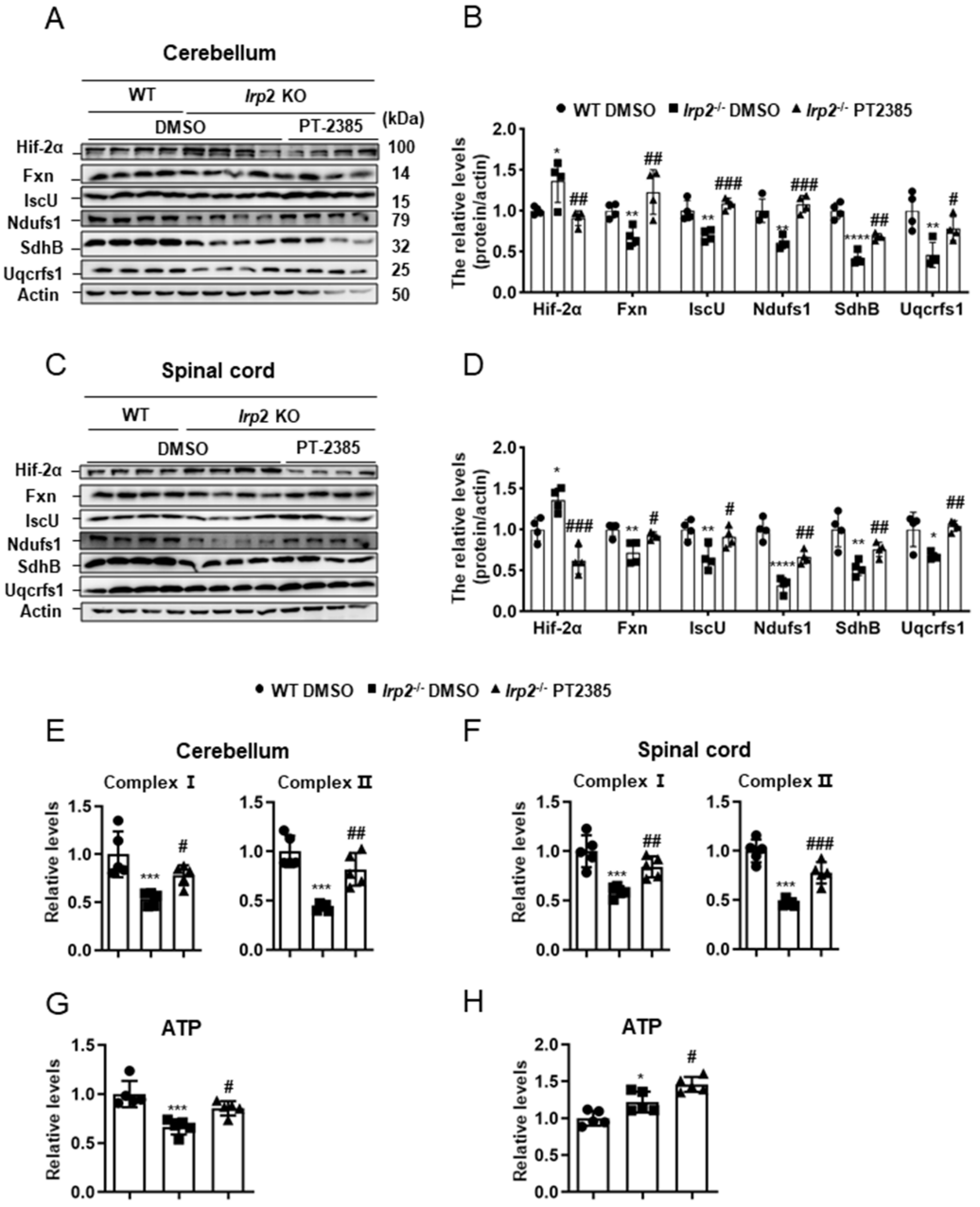

Figure 4

Inhibition of Hif2α by PT-2385 effectively rescues mitochondrial function in the cerebellum and spinal cord of Irp2-/- mice. (A) Protein levels of Fe–S biogenesis-related genes (Fxn and IscU) and mitochondrial complex subunits (Ndufs1, SdhB and Uqcrfs1) in the cerebellum detected by Western blot analysis. Actin was used as an internal control. (B) Quantification of the band intensity for (A). (C) The same proteins as in (A) in the spinal cord detected by Western blot analysis. Actin was used as an internal control. (D) Quantification of the band intensity for (C). (E, F) Activities of ETC complexes I and II of the cerebellum (E) and spinal cord (F). (G, H) The ATP content in the cerebellum (G) and spinal cord (H). Values represented the mean ± SEM n=3-5, and the ANOVA used for statistics to evaluate the group differences. In B, D, E, F, G and H, *P <0.05, **P <0.01, ***P <0.001, ****P <0.001, Irp2-/- DMSO vs. WT DMSO; #P <0.05, ##P <0.01, ###P <0.001, Irp2-/- PT-2385 vs. Irp2-/- DMSO.

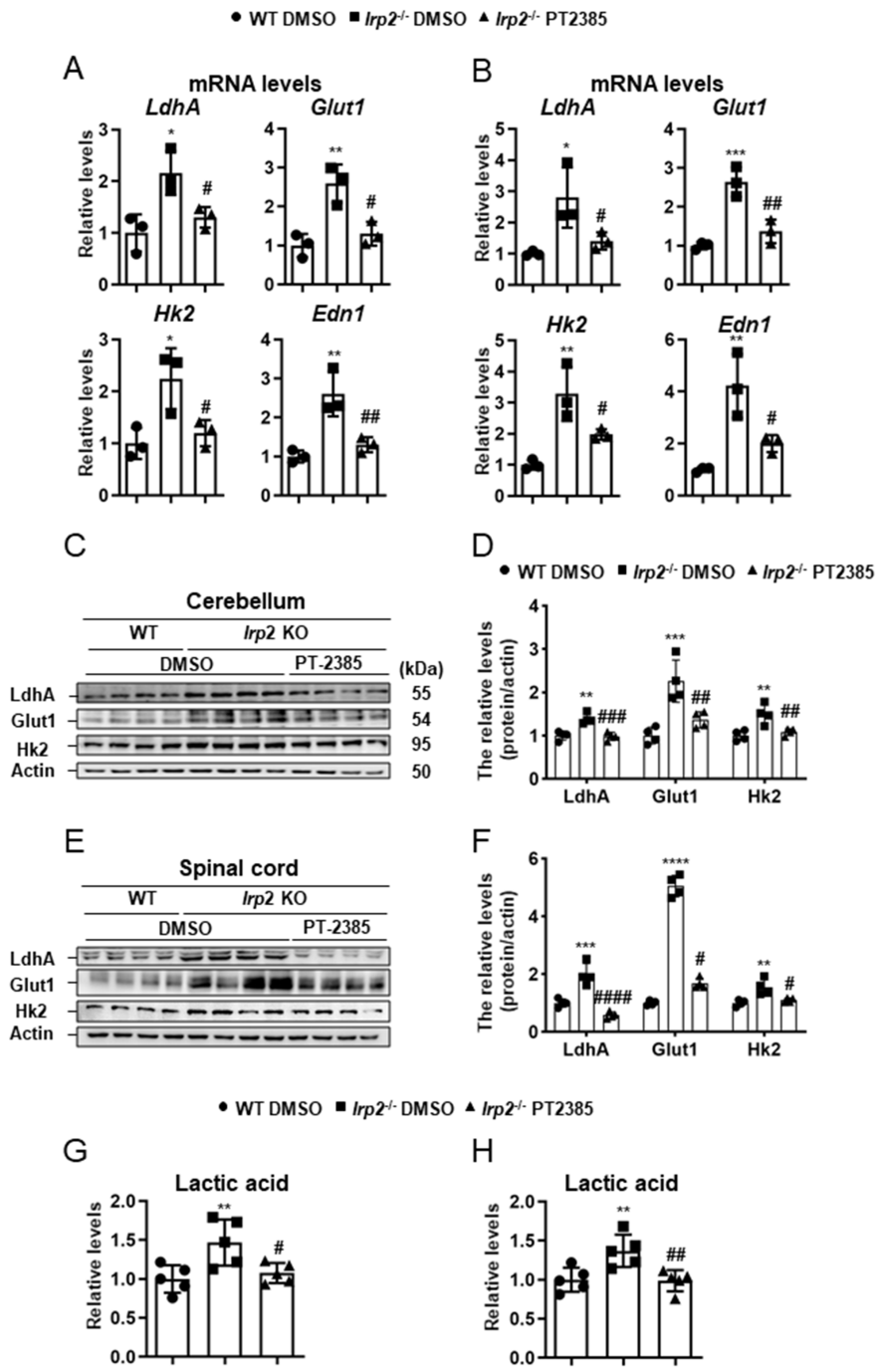

Figure 5

Inhibition of Hif2α by PT-2385 attenuates the enhanced glycolysis in the cerebellum and spinal cord of Irp2-/- mice. (A, B) The mRNA levels of Hif-target genes LdhA, Glut1, Hk2 and Edn1 in the cerebellum (A) and spinal cord (B), detected by qPCR. (C) Glycolytic pathway-related proteins (Glut1, Hk2, LdhA) in the cerebellum detected by Western blot analysis. Actin was used as an internal control. (D) Quantification of the band intensity for (C). (E) The same proteins as in (C) in the spinal cord detected by Western blot

analysis. Actin was used as an internal control. (F) Quantification of the band intensity for (E). (G, H) The lactic acid levels in the cerebellum (G) and spinal cord (H). Values represented the mean ± SEM, n=3-5. The ANOVA was used for statistics to evaluate the group differences. In A, B, D, F, G and H, *P <0.05, **P <0.01, ***P <0.001, Irp2-/- DMSO vs. WT DMSO; #P <0.05, ##P <0.01, ###P <0.001, ####P <0.0001, Irp2-/- PT-2385 vs. Irp2-/- DMSO.

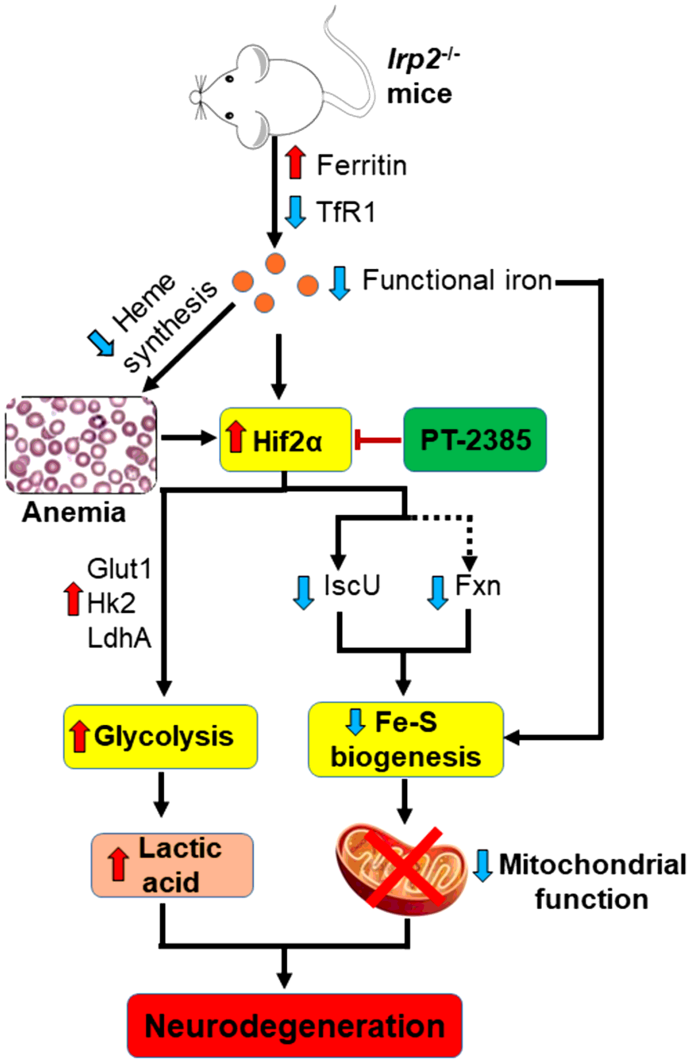

Figure 6

A working model to illustrate the potential target, Hif2a, in the therapeutic application of Irp2 loss-triggered neurodegenerative syndrome. Irp2 depletion causes the deficiency of cellular functional iron by decreased transferrin receptor and increased ferritin, which compromise the heme biosynthesis and finally trigger microcytic anemia in mice. Both the iron deficiency and anemia/hypoxia upregulate Hif2α expression in vivo. The elevated Hif2α upregulates glycolytic pathway-related genes to enhance glycolysis, while down-regulates iron-sulfur cluster biogenesis-related genes, Fxn and IscU, to weaken mitochondrial function. After the inhibition of Hif2α by PT-2385, the energy metabolism is shifted from glycolysis to oxidative phosphorylation in Irp2-/- mice and neurodegenerative symptoms are alleviated.